Zinc distribution and speciation in Arabidopsis *halleri* × *Arabidopsis lyrata* progenies presenting various zinc accumulation capacities

Géraldine Sarret[1], Glenda Willems[2], Marie-Pierre Isaure[1], Matthew A. Marcus[3], Sirine C. Fakra[3], Hélène Frérot[2], Sébastien Pairis[4], Nicolas Geoffroy[1], Alain Manceau[1] and Pierre Saumitou-Laprade[2]

[1]Environmental Geochemistry Group, LGIT, University J. Fourier and CNRS, BP 53, 38041 Grenoble Cedex 9, France; [2]Laboratoire de Génétique et Evolution des Populations Végétales, UMR 8016, CNRS, Université Lille 1, F–59655 Villeneuve d'Ascq, France; [3]Advanced Light Source, Lawrence Berkeley Lab, 1 Cyclotron Road, Berkeley, CA 94720, USA; [4]Institut Néel CNRS-UJF, Dept Matière Condensée, Matériaux et Fonctions, Pôle Instrumentation, 25 av. des Martyrs, BP 166, F–38042 Grenoble Cedex 9, France

Author for correspondence:
Géraldine Sarret
Tel: +33 476 63 51 99
Email: geraldine.sarret@ujf-grenoble.fr

Key words: *Arabidopsis halleri*, *Arabidopsis lyrata*, extended X-ray absorption fine structure (EXAFS) spectroscopy, interspecific crossing, micro X-ray fluorescence (μXRF), scanning electron microscopy coupled to energy dispersive X-ray analysis (SEM-EDX).

Summary

- The purpose of this study was to investigate the relationship between the chemical form and localization of zinc (Zn) in plant leaves and their Zn accumulation capacity.
- An interspecific cross between *Arabidopsis halleri* sp. *halleri* and *Arabidopsis lyrata* sp. *petrea* segregating for Zn accumulation was used. Zinc (Zn) speciation and Zn distribution in the leaves of the parent plants and of selected F_1 and F_2 progenies were investigated by spectroscopic and microscopic techniques and chemical analyses.
- A correlation was observed between the proportion of Zn being in octahedral coordination complexed to organic acids and free in solution (Zn–OAs + Zn_{aq}) and Zn content in the leaves. This pool varied between 40% and 80% of total leaf Zn depending on the plant studied. Elemental mapping of the leaves revealed different Zn partitioning between the veins and the leaf tissue. The vein : tissue fluorescence ratio was negatively correlated with Zn accumulation.
- The higher proportion of Zn–OAs + Zn_{aq} and the depletion of the veins in the stronger accumulators are attributed to a higher xylem unloading and vacuolar sequestration in the leaf cells. Elemental distributions in the trichomes were also investigated, and results support the role of carboxyl and/or hydroxyl groups as major Zn ligands in these cells.

Introduction

Recently, great attention has been given to the metal hyperaccumulator *Arabidopsis halleri* (Broadley *et al.*, 2007 and references therein). *Arabidopsis halleri* is a pseudo-metallophyte species, thus occurring on both contaminated and noncontaminated sites. Based on a survey of 33 metallicolous and nonmetallicolous populations, *A. halleri* was defined as constitutively zinc (Zn) tolerant, though displaying minor quantitative variations in Zn tolerance levels depending on the origin of the population (Pauwels *et al.*, 2006). In addition, as a Zn hyperaccumulator, *A. halleri* can concentrate Zn in extremely high amounts in its aerial parts. This species is phylogenetically close to the model species *Arabidopsis thaliana*, which implies that the resources and tools developed for *A. thaliana* can be used to study the genetic and physiological mechanisms underlying metal tolerance and hyperaccumulation in *A. halleri*. Thanks to several interesting characteristics (genetic proximity to *A. thaliana*, presence of plants in contaminated and non contaminated areas, widespread distribution in Europe, etc.), *A. halleri* is considered an appropriate model plant for studying metal tolerance and hyperaccumulation (Roosens *et al.*, 2008a).

Much effort has been made to improve our understanding of the origin and evolutionary dynamics of metal tolerance and accumulation (Macnair, 2002; Van-Rossum *et al.*, 2004; Pauwels *et al.*, 2005, 2006; Koch &

Matschinger, 2007). Although *A. halleri* is self-incompatible, interspecific crossings are possible between *A. halleri* and its non tolerant and non hyperaccumulating relative *Arabidopsis lyrata* ssp. *petraea* (henceforth *A. lyrata*) (Macnair *et al.*, 1999). The genetic analysis of Zn tolerance and accumulation in *A. halleri* was initiated by the use of such interspecific crosses through which the constitutive nature of Zn tolerance in *A. halleri* could be bypassed (Macnair *et al.*, 1999). Based on the segregation of Zn tolerance and Zn accumulation in the F_2 progeny, the authors concluded that both traits were dominant and genetically independent in *A. halleri*. Recently, an *A. halleri* × *A. lyrata* first-generation backcross progeny (BC1) was used to elucidate the genetic architecture of Zn tolerance in *A. halleri*. Three quantitative trait loci (QTLs) of comparable additive effect were found to govern Zn tolerance in *A. halleri* (Willems *et al.*, 2007). Interestingly an independent phenotyping analysis for Zn accumulation performed on the same BC1 showed a recessive component of the trait and detected a QTL (ZnAcc1) that colocalized with Zn tolerance (Roosens *et al.*, 2008b). Other studies aimed at identifying genes involved in metal uptake and protection against metal toxicity. Through transcription profiling and comparison of genes expression in *A. halleri* and in *A. thaliana*, a wide range of genes known to be involved in metal homeostasis in *A. thaliana* were identified as being potentially related to metal tolerance and hyperaccumulation in *A. halleri* (Becher *et al.*, 2004; Drager *et al.*, 2004; Weber *et al.*, 2004; Dräger *et al.*, 2005; Chiang *et al.*, 2006; Elbaz *et al.*, 2006; Talke *et al.*, 2006). Recently, a comparative genomics analysis with *A. thaliana* demonstrated that the heavy metal transporter HMA4 was the single candidate gene included in the ZnAcc1 QTL region in *A. halleri* (Roosens *et al.*, 2008b). A functional analysis performed for this gene showed that it contributed significantly to Zn tolerance and hyperaccumulation in *A. halleri* (Hanikenne *et al.*, 2008). In addition to these genetic and physiological studies, microscopic and spectroscopic tools have been used to analyse the fate of Zn, that is, the localization and the chemical form of this metal, in the leaves of hyperaccumulating species. In *A. halleri*, the major Zn storage compartment is the mesophyll tissue (Küpper *et al.*, 2000; Zhao *et al.*, 2000). At the cellular level, a vacuolar sequestration of metals, as shown for the Zn and Cd hyperaccumulator *Thlaspi caerulescens* (Küpper *et al.*, 1999; Frey *et al.*, 2000), has also been suggested for *A. halleri* (Küpper *et al.*, 2000). Whereas Zn occurs as Zn phosphate in the non tolerant and non hyperaccumulating species *Arabidopsis lyrata*, the major chemical form of Zn in *A. halleri* leaves identified by extended X-ray absorption fine structure (EXAFS) spectroscopy was Zn malate (Sarret *et al.*, 2002). Trichomes were also found to exhibit extremely high metal concentrations at their base (Küpper *et al.*, 2000; Zhao *et al.*, 2000; Sarret *et al.*, 2002). Trichomes of *A. halleri* are unicellular and non glandular. Their possible role in metals detoxification remains unclear.

Thanks to the fact that the F_1 and F_2 progenies of *A. halleri* × *A. lyrata* crossings show a variety of Zn accumulation patterns, it is possible to study the relationship between the capacity of Zn accumulation and the fate of Zn in the leaves. The distribution of metals in plants can be studied by various imaging techniques using electrons, particles or X-ray beams (Lobinski *et al.*, 2006). Micro X-ray fluorescence (μXRF) offers the advantages of a relatively high sensitivity (a few ppm), an increased penetration depth compared with particles and electrons, and the possibility to map large areas such as portions of leaves within a reasonable time. Extended X-ray absorption fine structure spectroscopy is a proven powerful tool to probe the chemical form of metals in plants (Salt *et al.*, 2002). Although it provides precise information on the nature and geometry of the metal-binding sites, in the case of metal-organic complexes it is generally unable to identify the molecule that the binding sites belongs to, except for ligands with strong signatures such as oxalate or histidine. The nature of organic ligands is even more difficult to determine when the metal is bound to several of those. Hence, it is useful to couple X-ray spectroscopy with chemical analyses of candidate metal ligands.

In this work, a set of plants including *A. halleri*, *A. lyrata* and their F_1 and F_2 progenies exhibiting a range of Zn accumulation phenotypes were selected. The distribution of Zn in the leaves was investigated by μXRF and scanning electron microscopy coupled to energy dispersive X-ray analysis (SEM-EDX), and the chemical form(s) of Zn were determined by Zn K-edge EXAFS spectroscopy and organic acids profiling. These results were then compared with Zn accumulation phenotypes.

Materials and Methods

Plant material

Arabidopsis halleri (L.) O'Kane & Al-Shehbaz individuals originated from an industrial site in the North of France (Courcelles) contaminated with Zn, cadmium (Cd) and lead (Pb), and *A. lyrata* (O'Kane & Al-Shehbaz) individuals from a nonpolluted site in the Czech Republic (Unhošt', Central Bohemia) were kindly provided by Prof. M. Macnair. The parent plants and the F_1 progeny produced by interspecific cross have been described previously (Willems *et al.*, 2007). Because *A. halleri* and *A. lyrata* are strongly allogamous species, the *A. halleri* × *A. lyrata* F_2 progeny was developed from two independent *A. halleri* × *A. lyrata* crosses in order to avoid inbreeding depression in progenies. Two F_1 individuals, one from each cross, were randomly chosen and crossed reciprocally to produce an F_2 generation of 288 progenies for QTL analysis of Zn

Table 1 Zinc accumulation phenotypes and analyses performed for each Arabidopsis plant

	Zn accumulation (μmol g^{-1} DW)	Chemical analyses	Physical analyses
Arabidopsis halleri	97.9	Zn, Fe, Mn, P, Mg, K, Ca, Si and OAs	Zn EXAFS and μXRF
Arabidopsis lyrata	6.6	Zn, Fe, Mn, P, Mg, K, Ca, Si and OAs	Zn EXAFS and μXRF
$F_{1\text{-}1}$	17.7	Zn, Fe, Mn, P, Mg, K, Ca, Si and OAs	Zn EXAFS and μXRF
$F_{1\text{-}2}$	43.9	Zn and OAs	Zn EXAFS
$F_{2\text{-}1}$	18.2	Zn and OAs	Zn EXAFS
$F_{2\text{-}2}$	28.0	Zn and OAs	Zn EXAFS
$F_{2\text{-}3}$	12.2	Zn, Fe, Mn, P, Mg, K, Ca and Si	μXRF
$F_{2\text{-}4}$	30.8	Zn and OAs	μXRF
$F_{2\text{-}5}$	60.6	Zn and OAs	Zn EXAFS
$F_{2\text{-}6}$	59.2	Zn, Fe, Mn, P, Mg, K, Ca and Si	μXRF
$F_{2\text{-}7}$	79.5	Zn and OAs	Zn EXAFS
$F_{2\text{-}8}$	170.8	Zn, Fe, Mn, P, Mg, K, Ca and Si	μXRF
$F_{2\text{-}9}$	83.0	Zn and OAs	Zn EXAFS
$F_{2\text{-}10}$	98.0	Zn and OAs	Zn EXAFS

The plants selected for extended X-ray absorption fine structure (EXAFS) and micro X-ray fluorescence (μXRF) analyses are not the same because these experiments were performed at different times, and not all the phenotypes of the F_2 progenies (288 in total) were known at those times. OAs, Organic acids.

accumulation (H. Frérot, unpublished). A few of them were selected for this study (Table 1).

Production of plants for EXAFS, μXRF and chemical analyses

All plants were grown individually in 1-L pots containing compost, in glasshouse environment (temperature, 20°C d : 15°C night; light, 14 h d^{-1}). The photoperiod was adjusted by 400 W high-pressure sodium lamps (photosynthetically active radiation (PAR): 90 µmol of photons m^{-2} s^{-1} over the wavelength range 400–700 nm); the lamps were automatically switched off when daylight was sufficiently intense. The humidity was not controlled but the experiment was performed in February, so the humidity was relatively stable in the glasshouse. Plants were watered every 2 d with deionized water.

Three replicates of each individual were obtained by vegetative propagation. Cuttings were grown for 4 wk in non-contaminated compost for rooting, and then for 5 wk in compost containing 500 mg Zn provided as $ZnSO_4$ per kilogram of fresh compost. Because of the limited available synchrotron beamtime, triplicate analyses were not possible for EXAFS and µXRF. Therefore, after harvesting the mature leaves, the three replicates were pooled. This pooling provided enough material to perform EXAFS, µXRF and chemical analyses on the same sample. Pooled plants were immediately immersed in liquid N_2. For each sample, one portion of the material was ground and pressed as 5 mm diameter pellet in liquid N_2 and the frozen pellet was stored in a liquid N_2 container until EXAFS measurements, another part was freeze-dried and kept intact for µXRF and SEM-EDX investigations, and the rest was freeze-dried and ground before chemical analyses. In addition, mature leaves of *A. halleri* grown in the same conditions were dried at 40°C and trichomes were collected using a clean razorblade for chemical analyses.

Chemical analyses

The plant material was analysed at the Service Central d'Analyses (USR-59/CNRS, Vernaison, France). For total elemental contents, leaf and trichome powders were digested with HNO_3/$HClO_4$ [80 : 20 (v : v)] and elemental concentrations were determined using inductively coupled plasma–atomic emission spectrometry (ICP-AES). For the total content in malate, malonate, citrate, succinate, oxalate and isocitrate, leaf powders were placed in a 0.1 N HCl solution and ultrasonicated for 1 h to extract and dissociate the Zn–OAs complexes. The suspension was then filtered at 0.45 µm, and cations were extracted from the solution using a cationic exchange resin (On Guard H; Dionex, Sunnyvale, CA, USA). The solution was then neutralized to pH 7.0 ± 0.1 using a 1 N NaOH solution. The OAs concentrations were measured by ionic chromatography (Dionex DX500) equipped with a conductimetric detection, using a column AS11-HC with a 1–40 mM NaOH gradient as eluant.

Scanning electron microscopy coupled to energy dispersive X-ray analysis

Freeze-dried leaves and isolated trichomes of *A. halleri* and *A. lyrata* were mounted on carbon stubs using carbon tape and coated with carbon. Samples were imaged and analysed using a scanning electron microscope (Jeol-JSM840A, Jeol, Tokyo, Japan) equipped with an EDX system (Kevex Si(Li)

diode, Kevex, Scotts Valley, Ca, USA) with a chamber pressure of 10^{-6}–10^{-5} Torr, and an accelerating voltage of 20 kV. The EDX profiles along trichomes and EDX spectra on chosen spots were recorded. For semi-quantification, spectra were analysed by applying ZAF calculation (IDFIX software, SAMx, St Laurent, France). Five trichome profiles were recorded for each species.

Micro-X-ray fluorescence

Micro-XRF mapping of the distribution of Zn and other elements in the leaves was performed on beamline 10.3.2 of the Advanced Light Source, Lawrence Berkeley National Laboratory, Berkeley, CA, USA (Marcus *et al.*, 2004). Fragments of freeze-dried leaves were fixed with aluminum tape on an *x*–*y* translation stage, and scanned under a microfocused beam. Coarse maps were first recorded using a 16 μm (H) × 7 μm (V) beam, and then finer maps on regions of interest were recorded using a 5 μm (H) × 5 μm (V) beam. The incident energy was set at 10 keV. The fluorescence yield was measured with a seven-element germanium (Ge) solid-state detector and normalized by I_0 and the dwell time. The vein : tissue fluorescence ratio was calculated on eight maps for *A. halleri*, three for *A. lyrata*, and one for the $F_{1\text{-}1}$, $F_{2\text{-}3}$, $F_{2\text{-}4}$, $F_{2\text{-}6}$ and $F_{2\text{-}8}$ plants. For each map, five regions were selected, and in each one the vein : tissue fluorescence ratio was obtained by dividing the normalized Zn counts measured in the vein by those measured in the tissue at *c.* 300 μm from the vein. Values presented are averages of the ratios obtained from the various regions and maps.

EXAFS data acquisition and analysis

The preparation of Zn model compounds is detailed in the Supporting Information, Methods S1. Zinc K-edge bulk EXAFS spectra for the plant leaves and reference compounds were recorded on the FAME Beamline at the European Synchrotron Radiation Facility (ESRF, Grenoble, France). Pellets of frozen-hydrated leaves and reference compounds were transferred to a He cryostat and cooled to 15 K. Spectra were recorded in fluorescence mode using a Si(220) double crystal monochromator and a 30-element solid-state Ge detector (Canberra, Lingolsheim, France). For each sample, three to eight scans of 40 min each, depending on Zn concentration, were averaged. Some reference spectra described previously (Sarret *et al.*, 2002; Panfili *et al.*, 2005) were recorded at room temperature. The normalization of the EXAFS spectra was performed according to standard methods. The k^3-weighted EXAFS spectra recorded on the plants were least-squares fitted over a wave vector (k) range of 2.0–11.5 $Å^{-1}$ using a combination of Zn standards from a library of Zn model compounds described earlier. The best fits, defined by normalized sum-squares residual ($NSS = \sum[k^3 \chi_{exp} - k^3 \chi_{fit}]2/\sum[k^3 \chi_{exp}]^2\ 100$), which is between the value obtained for the best fit (NSS_{best}) and 1.05 NSS_{best}, was used to calculate the mean and standard deviation of each component. In parallel, the structural parameters for the first and second Zn coordination shells were determined with simulations using ARTEMIS (Ravel & Newville, 2005). The EXAFS spectra were Fourier transformed over a k range of 3.5–11.5 $Å^{-1}$, and the contribution of the first and second shell was simulated in k and R space. Phase and amplitude functions were calculated by FEFF6 (Rehr *et al.*, 1991) from the structures of Zn malate dihydrate (Reed & Karipides, 1976) for Zn–O and Zn–C pairs, Zn histidine dihydrate (Kistenmacher, 1972) for Zn–N and Zn–C pairs, and hopeite (Whitaker, 1975) for Zn–O, Zn–P and Zn–Zn pairs.

Statistical analyses

Correlations between variables were evaluated using the Spearman's rank correlation test (correlation coefficient R_S) with P set at 0.05. For the correlation between Zn accumulation and the proportion of Zn species determined by EXAFS, the test was performed on all the proportions determined after normalization of the sum of the percentages to 100%.

Results

Zn and organic acids content

The plants grown for 5 wk on compost containing 500 mg kg^{-1} Zn were analysed for Zn content in the leaves (Table 1). The F_1 hybrids showed Zn accumulation levels intermediate between *A. halleri* and *A. lyrata*, but relatively contrasted (17.7 and 43.9 μmol g^{-1} DW). This divergence might be because of the genetic heterogeneity in parental individuals used to generate both interspecific hybrids. The F_2 plants showed a range of Zn accumulation from 12.2 to 170.8 μmol g^{-1} DW, with one F_2 plant ($F_{2\text{-}8}$) showing a transgressive behavior.

The subset of plants studied by EXAFS spectroscopy (parental species, two F_1 and six F_2 plants) were also analysed for six organic acids (OAs) in the leaves (Table 2). The three most concentrated OAs were malate, citrate and oxalate. For *A. halleri*, the concentrations were consistent with those measured previously in a plant cultivated in hydroponic culture (Sarret *et al.*, 2002), with malate as the most concentrated OA. In *A. lyrata* oxalate was predominant. The three OAs, especially citrate, were often higher in the progenies than in the parental plant species. The sum of the six OA concentrations was always higher than Zn concentration. As observed previously (Zhao *et al.*, 2000; Sarret *et al.*, 2002), no correlation was found between Zn accumulation and OA content in the leaves (Fig. 1). The

Table 2 Total zinc and organic acid concentrations in the Arabidopsis leaves (μmol g^{-1} DW)

	Zn	Malate	Malonate	Citrate	Succinate	Oxalate	Isocitrate	Total OA[a]
Arabidopsis halleri	97.9	120.81	1.73	19.78	1.27	18.44	Nm	162.03
A. lyrata	6.6	115.59	1.44	61.41	<0.9	197.71	<0.5	376.16
$F_{1\text{-}1}$	17.7	149.90	1.83	129.07	<0.9	67.76	<0.5	348.55
$F_{1\text{-}2}$	43.9	186.44	2.45	157.70	<0.9	106.63	0.73	453.95
$F_{2\text{-}1}$	18.2	259.53	1.04	173.83	<0.9	176.61	1.41	612.41
$F_{2\text{-}2}$	28.0	140.95	1.73	222.23	<0.9	89.97	1.41	456.29
$F_{2\text{-}5}$	60.6	202.10	2.98	232.64	<0.9	83.31	1.51	522.54
$F_{2\text{-}7}$	79.5	65.63	1.25	204.54	<0.9	141.06	0.87	413.35
$F_{2\text{-}9}$	83.0	93.22	1.49	143.65	<0.9	16.33	2.37	257.05
$F_{2\text{-}10}$	98.0	164.07	10.28	250.86	<0.9	23.33	5.47	454.00

Plants were grown for 5 wk in compost containing 500 mg kg^{-1} Zn as $ZnSO_4$.
[a]Total OA, sum of the six organic acids.

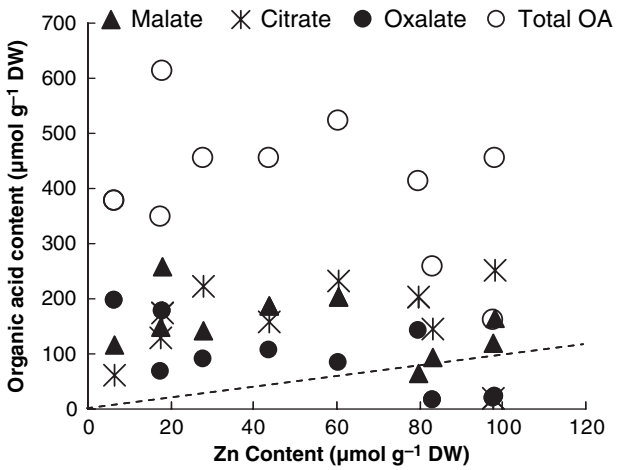

Fig. 1 Content of the three most concentrated organic acids (OAs) as a function of zinc (Zn) content in the leaves of the plants presented in Table 2. The line $y = x$ is drawn as indicator.

content of Fe, Mn, P, Mg, K, Ca and Si were measured in the leaves of the plants analysed by μXRF and no correlation was observed between the content of these elements and Zn accumulation (not shown).

Chemical form of Zn in the leaves

The chemical form of Zn in the leaves was investigated by Zn K-edge EXAFS spectroscopy. Fig. 2 shows the spectra for some candidate Zn species. The Zn local structure in these compounds was determined by shell simulations (Table 3). The spectra for aqueous Zn, Zn malate, Zn citrate, Zn succinate, Zn + 3 OAs (equimolar concentrations of malate, citrate and succinate) and Zn nicotianamine in solution have a similar frequency and slightly different shape of the second oscillation *c.* 6 $Å^{-1}$ (Fig. 2a). Other Zn–OAs in solution also display similar spectral signature (Fig. S1a). In all these samples, Zn is octahedrally coordinated, with Zn–O distances between 2.07 Å and 2.08 Å, as determined by shell simulations (Table 3). These species were grouped as 'Zn–OAs in solution and aqueous Zn^{2+}' (Zn–OAs + Zn_{aq}) in the linear combination fits. Zinc oxalate and Zn histidine have distinctive features on the second oscillation. The Zn–S interactions can be unambiguously distinguished from Zn–O and Zn–N interactions thanks to larger Zn–S bond distance (*c.* 2.35 Å) (not shown).

The spectra for Zn–cell wall and Zn-pectin have lower frequency oscillations than the ones of Zn–OAs and aqueous Zn^{2+} (Figs 2a and S1b), which reflects shorter Zn–O distances (2.00–2.02 Å, Table 3). These distances are intermediate between typical distances for octahedral (2.0–2.2 Å) and tetrahedral coordination (1.8–2.0 Å) (Sarret *et al.*, 1998). Therefore, Zn likely occupies both types of environments. The co-occurrence of octahedral and tetrahedral configurations is consistent with the lower amplitude of these two spectra relative to the Zn aqueous references. The Zn–cell wall and Zn-pectin spectra are roughly similar, which is not surprising since pectin is a likely Zn-binding component of plant cell walls. Indeed, this molecule contains carboxyl groups whereas cellulose and glycan, two other major components of the cell wall, contain hydroxyl groups only. In this study, Zn–cell wall and Zn-pectin spectra are used as proxies for Zn bound to the cell walls. The spectrum of ZnPhos (Zn-sorbed hydroxylapatite), used as a proxy for poorly crystallized Zn phosphate (Sarret *et al.*, 2004; Panfili *et al.*, 2005), presents low frequency oscillations as well. The Zn–O distance (1.97 Å) suggests a tetrahedral coordination. The higher shells were simulated by phosphorus (P) and Zn atoms at 2.94 and 3.30 Å, respectively (Table 3).

The Zn K-edge EXAFS spectra of the leaf samples are displayed in Fig. 3. We did not use principal component analysis because of the relatively small number of spectra and their similarity to each other. Instead, we performed linear combination fitting (LCF) to a library of standard spectra. For each spectrum, a single component was first tested, and an additional component was allowed if the fit quality was improved significantly, that is, if NSS was decreased by at least 10%. Using this procedure, all spectra

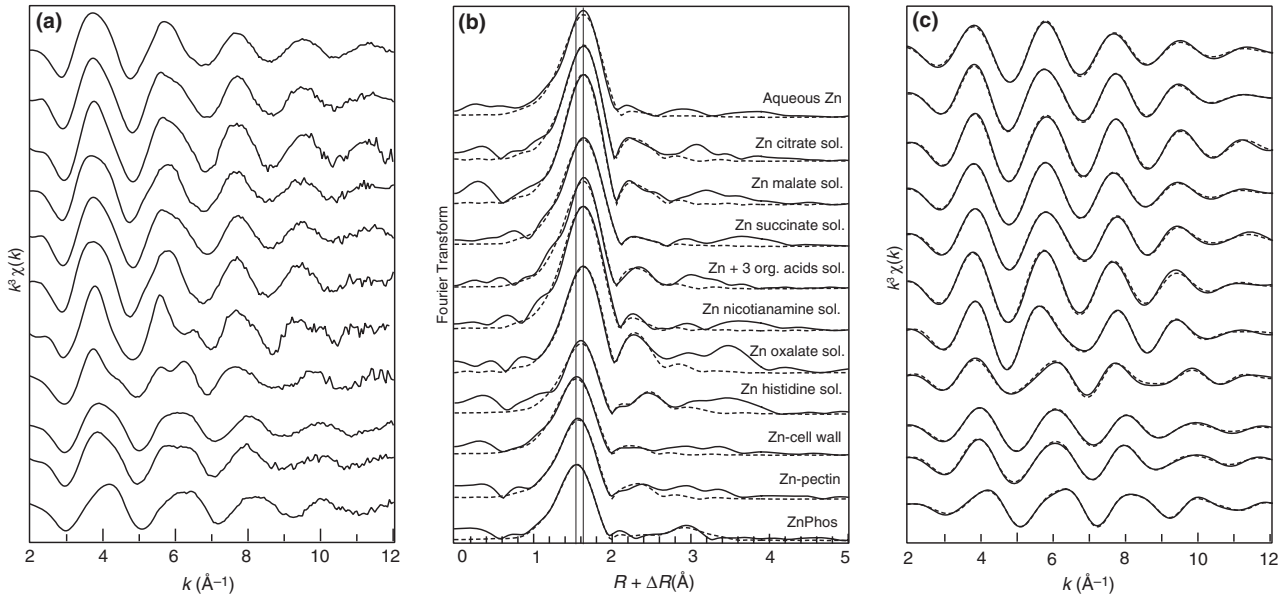

Fig. 2 Zinc (Zn) K-edge extended X-ray absorption fine structure (EXAFS) spectra (a), Fourier transforms (b) and back-transforms for the two first shells (c) and shell simulations for selected Zn species. Solid lines, experimental data; dashed lines, simulations. Samples include, from top to bottom: aqueous Zn (1 M $Zn(NO_3)_2$, pH 4.0), Zn citrate (10 mM $Zn(NO_3)_2$ + 100 mM citrate, pH 4.5), Zn malate (10 mM $Zn(NO_3)_2$ + 100 mM malate, pH 5.5), Zn succinate (10 mM $Zn(NO_3)_2$ + 100 mM succinate, pH 5.5), Zn + 3 organic acids (10 mM $Zn(NO_3)_2$ + 33 mM malate + 33 mM citrate + 33 mM succinate, pH 5.5), Zn nicotianamine (3 mM $Zn(NO_3)_2$ + 12 mM nicotianamine, pH not measured), Zn oxalate (33 mM $Zn(NO_3)_2$ +130 mM oxalate, pH 5.0), Zn histidine (10 mM $Zn(NO_3)_2$ + 100 mM histidine, pH 5.5), Zn–cell wall (Zn complexed to isolated tobacco (*Nicotiana tabacum*) root cell wall, 1.4 μmol Zn g^{-1} DW), Zn pectin (pectin containing 7.6 μmol Zn g^{-1} DW), and ZnPhos (Zn-sorbed hydroxylapatite containing 1% Zn, prepared at pH 5.0).

were correctly simulated by three components. Satisfactory fits were defined by NSS increase within 5% of that for the best fit. Using this criterion, 8–24 good fits were obtained depending on the sample. Table 4 presents the averages and standards deviations calculated on these good fits. Three types of components were identified, including Zn–OAs + Zn_{aq}, Zn–cell wall complexes (represented by Zn–cell wall or Zn-pectin) and Zn phosphate (represented by Zn-sorbed hydroxylapatite or Zn phytate). The proportions of these species in each sample are presented in Table 4. Zinc bound to thiol groups never showed up in the fits.

In our previous study performed on freeze-dried leaves of *A. halleri* (Sarret *et al.*, 2002), Zn malate (in solid state) was the unique Zn species identified. In the present study on frozen-hydrated leaves, the best single-component simulation, obtained with Zn malate in solution, was unsatisfactory (NSS = 16.8). Satisfactory fits were obtained with three components, including Zn malate in solution (30–40%), another Zn–OA standard in solution or aqueous Zn^{2+} (20–40)%, and either Zn phosphate (*c.* 20%) or Zn–cell wall (*c.* 30%) as third component (Table 4). If Zn malate was excluded, the residual was increased by 6% compared with the best fit. Therefore, malate is a likely but probably not unique ligand for Zn in *A. halleri* leaves. The presence of other OA(s) and their nature is not known because fits of equivalent quality were obtained with various references (succinate, citrate, lactate, mixture of three OAs, etc.) and with aqueous Zn^{2+}. The deviation between this study and our previous study might reflect some variability in Zn speciation between different culture conditions (hydroponics **vs** artificially contaminated soil). However, Zn malate was identified both in plants grown in hydroponics and collected in the field (Sarret *et al.*, 2002). A more likely reason for this disagreement is the freeze-drying treatment of the samples in our previous work, which might have altered Zn speciation (see the Discussion section). For *A. lyrata*, acceptable fits were obtained with a combination of Zn–cell wall (*c.* 50%), Zn–OAs + Zn_{aq} (*c.* 40%) and Zn phosphate (*c.* 25%). Contrary to the case for *A. halleri*, Zn malate was not more frequently observed in the fits than the other Zn–OA references. Note that the sum of the three components equals 115% whereas for other samples the sum equals 95% instead of 100%, so all percentages should be normalized to 100% before comparison. Such small discrepancies are usual in LCF using a limited number of model compound spectra to fit a complex system. Again, the Zn speciation in *A. lyrata* deviates from our previous study on freeze-dried leaves, in which phosphate was the unique Zn ligand (Sarret *et al.*, 2002). The spectrum for the non accumulator F_1 ($F_{1\text{-}1}$) was fitted with a combination of Zn–cell wall complexes and Zn–OAs + Zn_{aq}. For the other F_1 plant ($F_{1\text{-}2}$) and for all F_2 plants, Zn–OAs + Zn_{aq} were the major Zn species. Zinc malate showed up frequently in the LC fits, but other references (Zn citrate, Zn succinate, Zn + 3 OAs, etc.) also

Table 3 First and second shell structural parameters derived from the spectra shown in Fig. 2

Compound	Atom	*n*	*R* (Å)	σ^2	*NSS*
Aqueous Zn	O	6.0	2.08	0.008	0.83
Zn citrate sol.	O	6.2	2.07	0.008	0.47
	C	3.9	2.85	0.010	
Zn malate sol.	O	6.0	2.07	0.007	1.01
	C	2.8	2.86	0.010	
Zn succinate sol.	O	5.9	2.08	0.010	0. 69
	C	0.9	2.88	0.011	
Zn + 3 OA sol.	O	6.3	2.07	0.009	1.18
	C	3.5	2.85	0.010	
Zn nicotianamine sol.	O	6.6	2.08	0.008	1.27
	C	1.3	2.83	0.008	
Zn oxalate sol.	O	5.4	2.08	0.008	1.27
	C	6.7	2.83	0.009	
Zn histidine sol.	N	4.2	2.07	0.008	2.77
	O	1.2	2.65	0.008	
	C	5.4	2.96	0.009	
Zn–cell wall	O	4.6	2.00	0.010	0. 70
	C	1.3	2.83	0.010	
Zn pectin	O	4.9	2.02	0.010	0. 53
	C	2.4	2.86	0.010	
Zn-sorbed	O	3.8	1.97	0.008	0. 84
hydroxylapatite	P	0.4	2.94	0.010	
(ZnPhos)	Zn	4.3	3.30	0.011	

n, number of atoms; *R*, interatomic distance, σ^2: Debye Waller factor, NSS = $\sum[k^3\,\chi_{exp} - k^3\,\chi_{fit}]^2/\sum[k^3\,\chi_{exp}]^2$ 100, with *q* : Fourier filtered EXAFS signal. Experimental errors on *n* and *R* are *c*. 10% and 0.01 Å for the first shell, and 20% and 0.02 Å for the second shell, as estimated by the difference obtained on different spectra recorded on a similar sample. OAs, Organic acids.

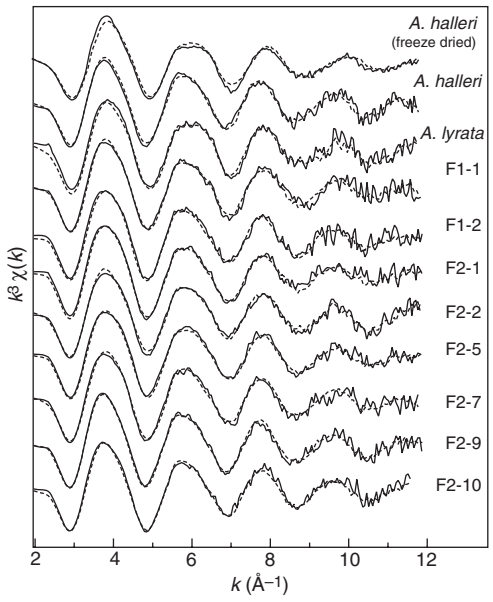

Fig. 3 Zinc (Zn) K-edge extended X-ray absorption fine structure (EXAFS) spectra for the plant leaves (solid lines) and best linear combination fits (dashed lines). All spectra were collected on frozen-hydrated samples except freeze-dried *Arabidopsis halleri* (denoted *A. h*-C, 250 μM in Sarret *et al*. (2002), fitted with 100% Zn malate (solid state).

provided good fits, so it was not possible to conclude on their exact nature. Secondary species included Zn–cell wall complexes and/or Zn phosphate, depending on the samples. The proportion of Zn–OAs + Zn_{aq} was slightly correlated with Zn total content in the leaves (R_S = 0.63, P = 0.05, Fig. 4). The proportion of the secondary Zn species (Zn–cell wall complexes or Zn phosphate) was not positively or negatively correlated with Zn content ($-0.41 < R_S < 0.22$, not shown).

In parallel with the LCF, the structural parameters for the first and second Zn coordination shells were determined by shell simulations (Fig. 5). All spectra were well-fitted with oxygen and carbon as nearest and next nearest atomic neighbors, respectively. Interatomic distances ranged from 2.03 to 2.07 Å for Zn–O, and from 2.79 to 2.92 Å for Zn–C (Table 5). The Zn–O distance was correlated with Zn content (R_S = 0.76, P = 0.05, Fig. 6). This indicates a higher proportion of Zn in octahedral coordination in the leaves presenting the highest Zn content. This is not surprising because Zn is sixfold coordinated in aqueous Zn–OA complexes and free Zn, six- and fourfold coordinated in Zn–cell wall complexes and fourfold in Zn phosphate references (Table 3). The correlation coefficient is higher for Zn accumulation **vs** Zn–O distance than for Zn accumulation **vs** percentage of Zn–OAs + Zn_{aq} (R_S = 0.76 and 63, respectively) probably because the first shell fits are less sensitive to the noise of the raw data than the linear combination fits. Both approaches lead to the same conclusion that is the proportion of aqueous Zn–OA complexes + free Zn is correlated with Zn accumulation in the leaves.

Distribution of Zn and other elements in the leaves

The elemental distribution in the plant leaves was studied by μXRF. Elements detected included silicon (Si), potassium (K), calcium (Ca), chromium (Cr), manganese (Mn), iron (Fe), cobalt (Co), nickel (Ni), copper (Cu) and Zn. Figure 7 compares the distribution of Zn, Mn and Ca in mature leaves of *A. halleri* and *A. lyrata*. In *A. halleri* the veins appear depleted in Zn relative to the surrounding leaf tissues. The attenuation length of the fluorescence signal at the energy of Zn K_α emission in an organic matrix is *c.* 1300 μm, and the thickness of the leaves is *c.* 500 μm maximum. Thus, the terms 'vein' and 'leaf tissue' include the internal tissues (vascular tissues and mesophyll, respectively) and the epidermis and cuticle. However, in *A. halleri* the epidermal cells are small and contain much less Zn than the mesophyll cells (Zhao *et al*., 2000), so most of the Zn fluorescence signal probably arises from the latter. The ratio of Zn fluorescence intensities between vein and leaf tissue is 0.8 ± 0.3 (Table 6). The leaf is twice as thick at the vein as it is in the surrounding leaf tissue, so the vein : tissue Zn concentration ratio can be roughly estimated as 0.4. As previously observed (Sarret *et al*., 2002),

Table 4 Proportions (in % mole fraction) of zinc species in the leaves determined by linear combination fitting (LCF)[a]

	Zn content (μmol g^{-1} dry weight)	Zn species (%)							
		Zn–OAs + Zn_{aq}	SD	Zn–cell wall	SD	Zn phosphate	SD	Sum	NSS_{best}[b] (%)
Arabidopsis halleri	97.9	75[a]	6			20	2	95	13.4
		66[b]	1	27	1			93	14.0
A. lyrata	6.6	41	4	49	7	25	4	115	7.3
$F_{1\text{-}1}$	17.7	50	4	57	3			107	7.8
$F_{1\text{-}2}$	43.9	76	4			28	4	104	7.8
		69	6	32	10			101	7.9
$F_{2\text{-}1}$	18.2	56	3	53	3			109	3.2
$F_{2\text{-}2}$	28.0	68	7	24	8	22	4	114	5.8
		73	4			36	2	109	5.9
		65	5	44	8			109	6.1
$F_{2\text{-}5}$	60.6	54	2	42	4	10	3	106	3.4
		51	2	54	1			105	3.4
$F_{2\text{-}7}$	79.5	54	1	53	2			107	4.6
$F_{2\text{-}9}$	83.0	87	1			15	2	102	4.8
		78	4	24	4			102	4.8
$F_{2\text{-}10}$	98.0	63	4	35	4			98	6.7
		76	6			26	2	102	6.9

[a]Average and standard deviation for the satisfactory fits, as defined by $NSS_{best} < NSS < 1.05\ NSS_{best}$. [b]Residual (normalized sum squares) for the best fit $NSS_{best} = \sum[k^3 \chi_{exp} - k^3 \chi_{fit}]^2 / \sum[k^3 \chi_{exp}]^2$ 100. [a]Including 41 ± 3% Zn malate. [b]Including 38 ± 1% Zn malate. OAs, Organic acids.

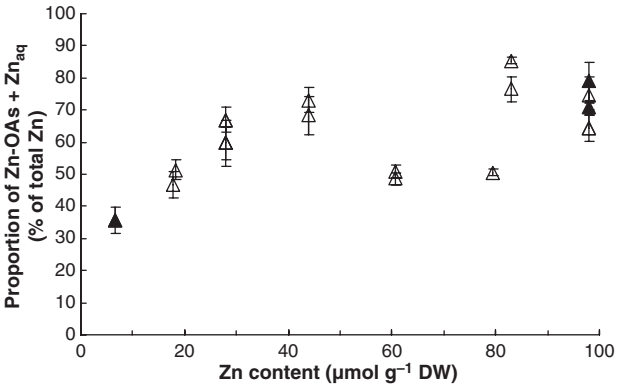

Fig. 4 Proportion of zinc (Zn)–organic acid complexes + aqueous Zn as determined by linear combination fittings (LCF) for the leaves of the parent, F_1 and F_2 plants as a function of Zn total content. Percentages presented in Table 4 were normalized to 100%. Closed symbols, parents; open symbols, progenies.

the most Zn-concentrated regions of the leaf are found at the base of the trichomes. The Zn distribution among the three compartments (leaf tissue, veins and trichomes) was estimated based on Zn fluorescence intensities and areas (Table 6). Zinc is mostly stored in the leaf tissue (76 ± 5% of total Zn). Despite their high Zn enrichment, trichomes accumulate only 10 ± 5% of total Zn. The contribution of the veins to Zn storage is roughly similar (14 ± 5% of total Zn).

The μXRF map for *A. lyrata* is almost a negative image of *A. halleri* (excluding trichomes), with a higher Zn signal in the veins than in the leaf tissue (Fig. 7b). The vein/leaf tissue Zn fluorescence ratio is 1.9 ± 0.3 (Table 6), therefore the vein : tissue Zn concentration ratio roughly equals 1. The leaf tissue is still the major Zn storage compartment, but contains only 54 ± 5% of total Zn compared with 76 ± 5% for *A. halleri*. The Zn distribution was also investigated in the leaves of an accumulator progeny (F2-8) and four non accumulator ones ($F_{1\text{-}1}$, $F_{2\text{-}3}$, $F_{2\text{-}4}$ and $F_{2\text{-}6}$). The former presents the same Zn depletion in the veins as *A. halleri* (Fig. 8; Table 6), whereas the latter shows a vein : tissue Zn ratio ≥ 1 (Fig. 9; Table 6). For all plants, the leaf tissue was always the major Zn storage compartment, accounting for 54–76% of total Zn. There was a significant negative correlation between the Zn content and the vein : tissue Zn counts ratio ($R_S = -0.71$, $P = 0.05$).

As previously observed (Küpper *et al.*, 2000; Zhao *et al.*, 2000; Sarret *et al.*, 2002), the trichomes of *A. halleri* show a Zn-enriched collar at their bases. The trichome base is also rich in Mn, Fe, Ni and Cu (Fig. S2), whereas Ca is more concentrated in the upper part of the trichomes (Fig. 10a). Similar metal accumulations are observed in the trichomes of *A. lyrata* and of the F_1 and F_2 progenies (Figs 10b,c and S3–S4). Other elemental distribution patterns are also observed within the trichomes, including a more diffuse accumulation of metals, or no metal enrichment at all (arrows in Figs 8 and 9). This does not seem to be related to the orientation of the trichomes towards the detector. No difference in elemental distribution between trichomes of young and mature leaves was observed.

To obtain further insights into the distribution of light elements, trichomes of *A. halleri* (Fig. 11) and *A. lyrata* (not shown) were also analysed by SEM-EDX. As observed by μXRF, Zn was generally concentrated in a 10–20 μm

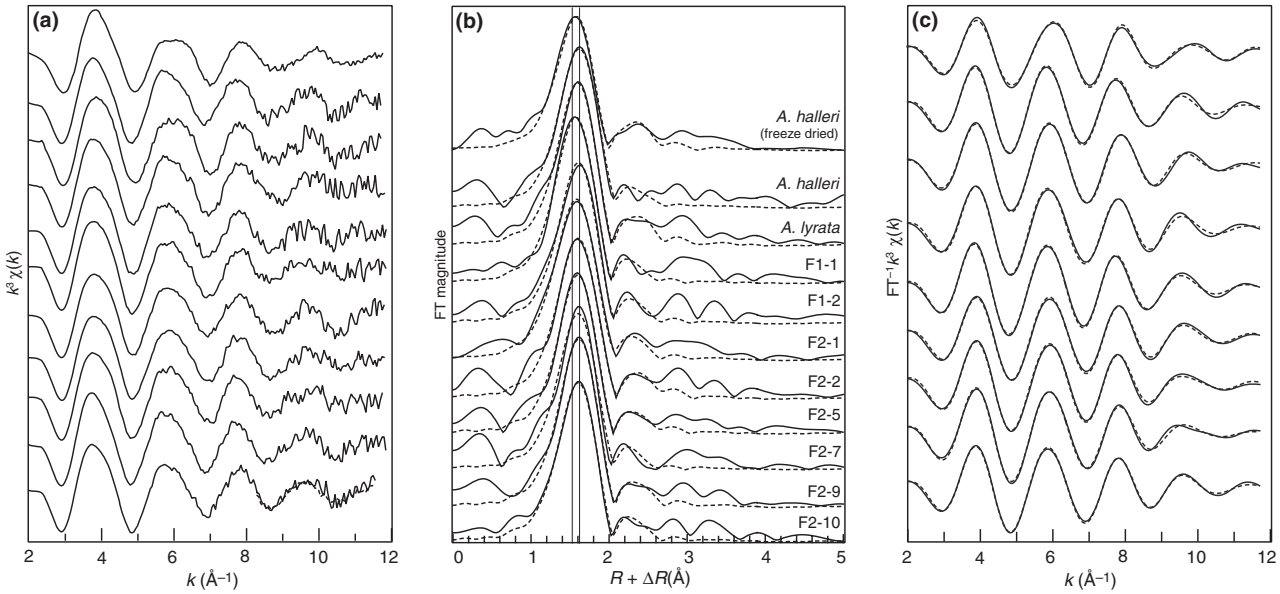

Fig. 5 Zinc (Zn) K-edge extended X-ray absorption fine structure (EXAFS) spectra recorded on plant leaves (a), Fourier transforms (b) and back-transforms for the first two shells (c). Solid lines, experimental data; dashed lines, simulations. All samples were analysed in the frozen-hydrated state except freeze-dried *Arabidopsis halleri* (sample *A. h*-C, 250 μM in Sarret *et al.* (2002).

Table 5 First and second shell structural parameters for the plant leaves

	Zn content (μmol g^{-1} DW)	Atom	*n*	*R* (Å)	σ^2	NSS
Arabidopsis halleri (freeze-dried)	160	O	4.5	2.02	0.010	1.64
		C	1.9	2.87	0.009	
A. halleri	97.9	O	5.9	2.07	0.010	1.50
		C	2.2	2.79	0.012	
Arabidopsis lyrata	6.6	O	6.0	2.03	0.010	1.44
		C	2.7	2.89	0.010	
$F_{1\text{-}1}$	17.7	O	5.6	2.04	0.010	0.51
		C	2.2	2.84	0.012	
$F_{1\text{-}2}$	43.9	O	5.9	2.06	0.010	1.06
		C	1.7	2.85	0.012	
$F_{2\text{-}1}$	18.2	O	5.9	2.05	0.012	0.41
		C	2.4	2.87	0.012	
$F_{2\text{-}2}$	28.0	O	5.9	2.05	0.010	1.11
		C	2.0	2.89	0.010	
$F_{2\text{-}5}$	60.6	O	5.9	2.05	0.010	0.86
		C	1.4	2.88	0.010	
$F_{2\text{-}7}$	79.5	O	4.7	2.05	0.008	1.45
		C	2.2	2.79	0.012	
$F_{2\text{-}9}$	83.0	O	6.3	2.07	0.010	0.76
		C	2.3	2.92	0.010	
$F_{2\text{-}10}$	98.0	O	5.9	2.07	0.010	0.34
		C	2.4	2.88	0.012	

The significance of the parameters and estimated experimental errors are given in the footnotes of Table 3. All spectra were recorded on frozen-hydrated samples except freeze-dried *Arabidopsis halleri*, denoted as sample *A. h*–C in (Sarret *et al.*, 2002), grown in 250 μM Zn.

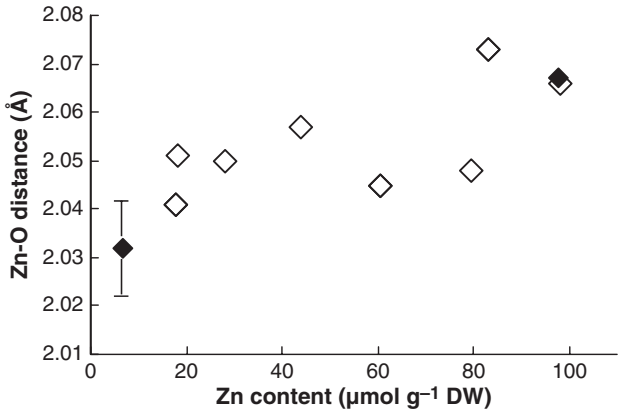

Fig. 6 Average first-shell zinc (Zn)–O distance determined by shell simulations as a function of Zn total content. The error bar corresponding to ± 0.01 Å is shown for one point. Closed symbols, parents; open symbols, progenies.

large ring in the lower part of the trichomes, and negatively correlated with Ca. An increased Si content was frequently observed in the Zn-rich region for both species, but this element was about threefold less concentrated than Zn. Sulfur was more concentrated at the base, and P was observed both at the base and upper parts of the trichomes. Again, no difference was observed between young and mature leaves. Finally, the total content in Mg, Si, P, K, Ca, Mn, Fe and Zn in isolated trichomes of *A. halleri* was determined by ICP-AES after digestion. Concentrations in μmol g^{-1} DW were 111 Mg, 24.9 Si, 100.1 P, 281 K, 1048 Ca, 18.2 Mn, 25.1 Fe and 275 Zn (i.e. 2.8-fold higher than bulk leaves). Therefore, despite the Si and Zn co localization on the ring, silanol groups can be excluded as major Zn ligands.

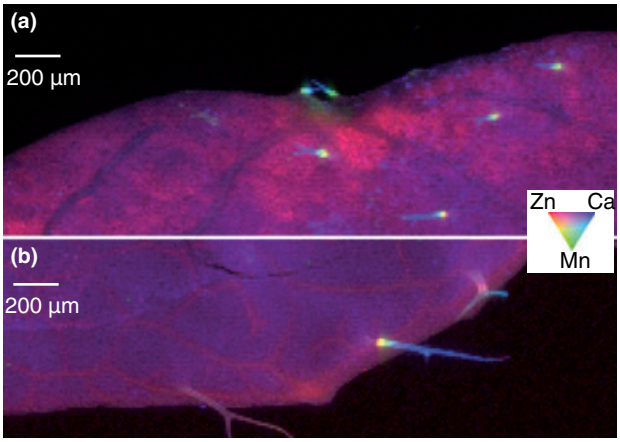

Fig. 7 Tricolor micro X-ray fluorescence (µXRF) maps of a portion of mature leaf of *Arabidopsis halleri* (a) and *Arabidopsis lyrata* (b) recorded at 10 keV, with 15 × 15 µm^2 pixel size and counting time of 50 ms pixel^{-1}. In *A. halleri* leaf, the veins appear depleted in zinc (Zn), whereas in *A. lyrata*, veins are richer in Zn.

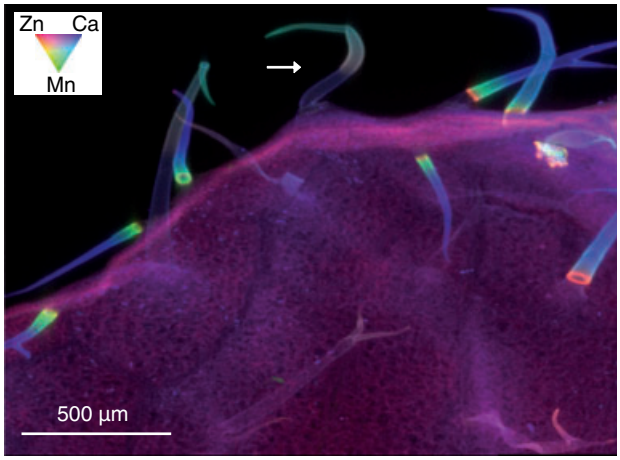

Fig. 8 Tricolor micro X-ray fluorescence (µXRF) maps of a portion of mature leaf of F_{2-8} recorded at 10 keV, with a 7 × 7 µm^2 pixel size and a counting time of 60 ms pixel^{-1}.

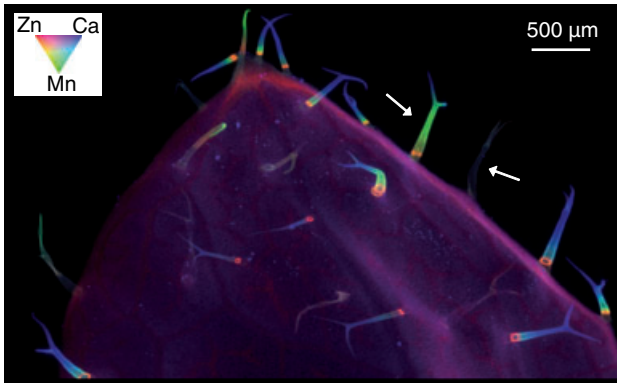

Fig. 9 Tricolor micro X-ray fluorescence (µXRF) maps of a portion of mature leaf of F_{2-6} recorded at 10 keV, with a 7 × 7 µm^2 pixel size and a counting time of 60 ms pixel^{-1}.

Phosphorus content is higher, but the EDX profile clearly shows that P is not colocalized with Zn.

Discussion

Segregating progenies from interspecific or intraspecific crosses have been widely used to study the relationships between metal tolerance and accumulation (Macnair *et al.*, 1999; Bert *et al.*, 2003; Zha *et al.*, 2004; Frérot *et al.*, 2005; Richau & Schat, 2009), the correlation between a given trait (accumulation, tolerance, root to shoot translocation, etc.) and gene expression (Dräger *et al.*, 2005; Hanikenne *et al.*, 2008; Xing *et al.*, 2008; Hassinen *et al.*, 2009), as well as to determine QTLs associated with metal tolerance and/or accumulation trait (Deniau *et al.*, 2006; Filatov *et al.*, 2007; Willems *et al.*, 2007; Roosens *et al.*, 2008a,b). The present study is the first to use spectroscopic and microscopic tools on these progenies with the aim of evaluating the relationship between Zn localization and speciation and Zn accumulation.

Our results showed that Zn was bound to oxygen-donor ligands in all plants. Three Zn species were identified: Zn–OAs + Zn_{aq}, Zn phosphate and Zn–cell wall complexes. The proportions of those three Zn species differed in the parent plants. In *A. halleri*, Zn malate complex represented 30–40% of total Zn. This organic acid was identified by

Table 6 Zinc distribution in the leaves as estimated by micro X-ray fluorescence (µXRF) on mature freeze-dried leaves

	Zn content (µmol g^{-1} DW)	Vein : tissue Zn counts[a]	Leaf Zn in each compartment[b] (%)		
			Leaf tissue	Veins	Trichomes
Arabidopsis halleri	97.9	0.8 ± 0.3	76 ± 5	14 ± 5	10 ± 5
Arabidopsis lyrata	6.6	1.9 ± 0.3	54 ± 5	26 ± 5	20 ± 5
F_{1-1}	17.7	2.3	57	34	9
F_{2-3}	12.2	1.0	64	16	20
F_{2-4}	30.8	1.8	54	25	21
F_{2-6}	59.2	1.6	58	24	18
F_{2-8}	170.8	0.6	73	11	16

[a]Ratio of the average Zn counts measured on the veins and on the leaf tissue. [b]Calculated by multiplying Zn counts by the estimated percentage of leaf surface occupied by each compartment (78% for the leaf tissue, 20% for the veins and 2% for the trichomes). This calculation assumes that µXRF at 10 keV probes the whole thickness of the leaf.

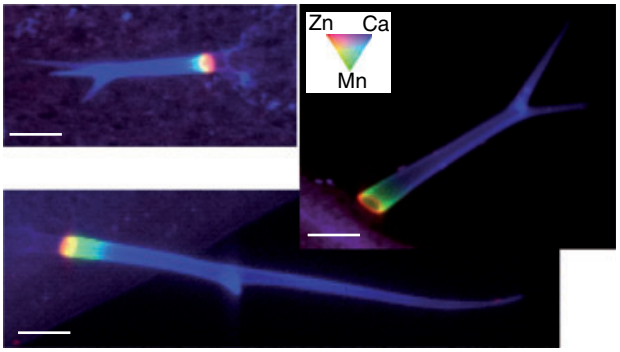

Fig. 10 Tricolor micro X-ray fluorescence (μXRF) maps of trichomes of *Arabidopsis halleri* (a), *Arabidopsis lyrata* (b) and F2-3 (c), recorded at 10 keV with 4 × 4 μm^2 pixel size for (a) and (b) and 3 × 3 μm^2 for C, and a counting time of 100 ms pixel^{-1}. Bars, 100 μm.

^{113}Cd nuclear magnetic resonance spectroscopy as the major ligand of cadmium in the leaves of *Thlaspi caerulescens* (Ueno *et al.*, 2005). Additional Zn species in the leaves of *A. halleri* included other Zn–OA complexes and aqueous Zn (20–40%), and Zn phosphate and/or Zn–cell wall complexes (20–30%). Although malate was the most concentrated OA among the six measured in this study, it has a weaker affinity for Zn than the other ones (Log K = 2.9 for malate compared with 4.0 and 4.5 for oxalate and citrate, respectively (Martell & Smith, 1982)). The speciation of Zn in solution was calculated with PhreeqC (Parkhurst & Appelo, 1999) using the complexation constants from Martell & Smith (1982) and the concentrations given in Table 1, supposing a factor of 100 between the concentrations in dry and fresh weight, and setting the pH at 5.5 which is the pH of the vacuoles. Calculated Zn species included 47% Zn^{2+}, 18% Zn malate, 18% Zn citrate, 13% Zn oxalate and 4% $Zn(malate)_2$. Thus, this very simple calculation is consistent with the presence of several Zn–OA complexes and free Zn^{2+}. Note that these percentages cannot be compared with the EXAFS percentages for two reasons. First, the calculation considers only Zn and the six organic acids as aqueous species in the same compartment and does not take into account the possible distribution between apoplasmic, cytoplasmic and vacuolar compartments. Second, in the Zn–OA references in solution, Zn is not present as a single Zn–OA complex but as a mixture of Zn^{2+} and Zn–OA, $Zn(OA)_2$, etc., depending on the OA considered.

We believe that the results obtained in the present study on frozen-hydrated state are more trustworthy that the results obtained previously on freeze-dried samples because dehydration may induce the precipitation of the species originally present in aqueous state. Such artifacts do not seem to be systematic, though, since relatively small changes have been observed in the case of Cd in *A. thaliana* (Isaure *et al.*, 2006). To date, the frozen-hydrated state and the

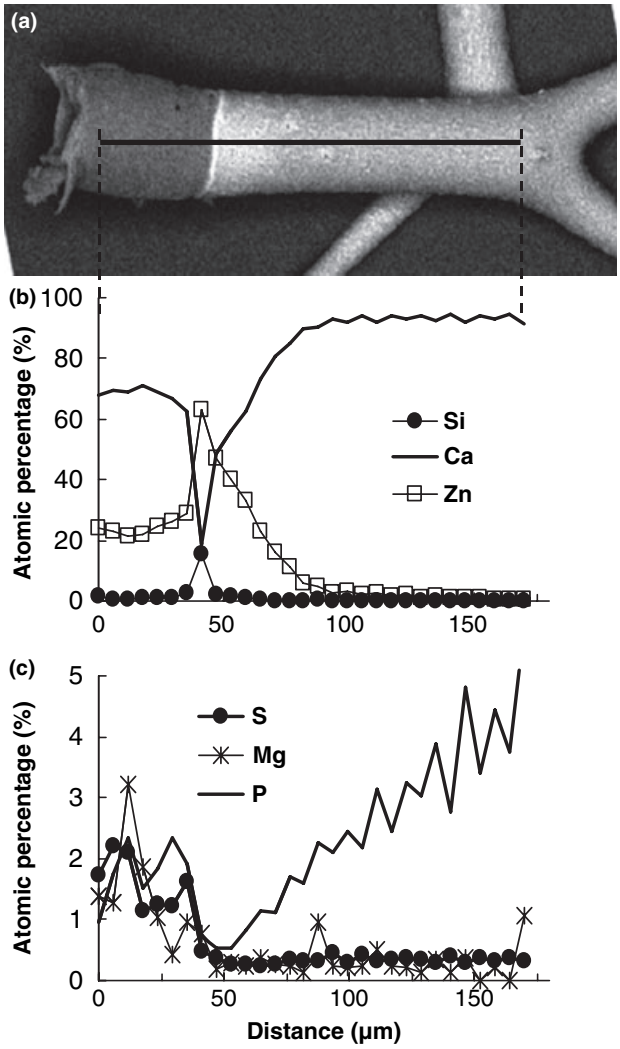

Fig. 11 (a) Back-scattered electron image of a trichome of *Arabidopsis halleri*. (b,c) Elemental profiles along the trichome obtained by scanning electron microscopy coupled to energy dispersive X-ray analysis (SEM-EDX). The atomic percentages were calculated using the ZAF method over the following elements: Mg, Si, P, S, Cl, K, Ca, Mn and Zn. C, N and O were not taken into account in the calculation.

measurement at low temperature (15 K in this experiment) are the least perturbing conditions for EXAFS data acquisition on biological samples (Küpper *et al.*, 2004; Ebbs *et al.*, 2009).

Arabidopsis lyrata contained less Zn–OAs + Zn_{aq} (*c.* 35%) and more Zn–cell wall complexes (*c.* 40%, percentages in Table 3 normalized to 100%). The proportion of these species also varied in the F_1 and F_2 plants.

For the whole set of plants studied, correlations were found between Zn accumulation and the proportion of Zn–OAs + Zn_{aq} (R_S = 0.63, P = 0.05) and between Zn accumulation and the first-shell Zn–O distance, which reflects the proportion of octahedral Zn (R_S = 0.76, P = 0.05). The vacuole of leaf cells has been shown to be a

major storage compartment of metals in the leaves of hyperaccumulating species, and OAs are often suggested as metal ligands in this compartment (Vazquez *et al.*, 1992; Brune *et al.*, 1994; Frey *et al.*, 2000; Küpper & Kroneck, 2005). Zn–OA complexes and free Zn might also be present in the xylem sap, as found in *Thlaspi* as secondary species (Salt *et al.*, 1999) and in rocket plants (*Eruca vesicaria*) (Terzano *et al.*, 2008). However, the xylem represents a largely minor Zn compartment compared with leaf cells. Therefore, the Zn–OAs and free Zn species identified by EXAFS might correspond to vacuolar Zn. In this hypothesis, 70–80% of Zn present in the leaves of *A. halleri* would be sequestered in the vacuoles, compared with *c.* 35% for *A. lyrata*. The localization of Zn phosphate is less clear. It might be present in the apoplasm (Van Belleghem *et al.*, 2007) or in the symplasm (Van Steveninck *et al.*, 1994).

Although the leaf tissue was the major accumulation compartment for all plants, differences in Zn partitioning between veins and tissue were observed. The vein : tissue Zn counts ratio was negatively correlated with Zn accumulation, suggesting enhanced transport of Zn from the vascular tissues to the leaf cells for the strongest accumulators.

A recent study showed that xylem loading in roots had an important role in the Zn hyperaccumulation process in *A. halleri*. The functional analysis of HMA4 in *A. halleri* and *A. thaliana* showed that silencing of *AhHMA4* by RNA interference completely suppressed Zn hyperaccumulation, which demonstrates clearly the key role of this protein in xylem loading and, consequently, in root-to-shoot translocation of Zn (Hanikenne *et al.*, 2008). However, the expression of AhHMA4 *in A. thaliana* resulted in a very low increase in shoot Zn concentration, suggesting that the expression of this protein in roots is not sufficient to realize Zn hyperaccumulation. Therefore, additional processes likely contribute to Zn hyperaccumulation. The sequestration in the vacuoles of root cells may limit the root-to-shoot transfer, as observed in *Thlaspi caerulescens* (Lasat *et al.*, 1998; Xing *et al.*, 2008; Richau *et al.*, 2009), whereas xylem unloading in the shoots and Zn sequestration in the vacuoles of leaf cells may contribute to this process (Palmgren *et al.*, 2008; Verbruggen *et al.*, 2009). Our results suggest a relationship between Zn accumulation and xylem unloading and vacuolar sequestration. It is not clear whether Zn accumulation is a cause or a consequence of these processes. The sequestration of Zn in the vacuoles might reduce its availability in the cells and favor Zn uptake and transfer, but alternatively a higher influx of Zn in the leaves might result in a stronger compartmentalization of the metal. The QTL analysis of Zn accumulation performed on the complete F_2 should clarify the role of HMA4 and additional genes or genomic regions and quantify their respective contribution in genetic variance explained (H. Frérot, unpublished).

In all plants investigated, most trichomes displayed a Zn-rich ring at their base. Metal sequestration in trichomes could be interpreted as an exclusion strategy limiting interferences with the metabolism of the mesophyll cells. However, trichomes account for only 10–20% of the total leaf Zn. Moreover, this mechanism does not seem to be related to metal tolerance and/or hyperaccumulation traits since it has been observed not only in metal-tolerant and hyperaccumulating species, including *A. halleri* (Küpper *et al.*, 2000; Zhao *et al.*, 2000; Sarret *et al.*, 2002) and *A. halleri* ssp. *gemmifera* (Hokura *et al.*, 2006; Fukuda *et al.*, 2008), but also in non tolerant and non accumulating species including *A. thaliana* (Ager *et al.*, 2003; Isaure *et al.*, 2006) and *A. lyrata* (this study). Moreover, the leaves of the Zn, Cd hyperaccumulator *T. caerulescens* do not contain trichomes. For *A. halleri*, some mature leaves devoid of trichomes were observed whereas young leaves were always covered by trichomes (not shown). Further analyses on *A. halleri* and other plants will be necessary to confirm the possible loss of trichomes during the life-cycle of the leaves. One may wonder whether the ring-like distribution pattern of metals could be an artifact of sample preparation. The dehydration of cells inevitably leads to a deposition of elements initially present in the vacuole or cytoplasm on the membranes. However, it is not clear why this would lead to a ring-like distribution of metals. Moreover, metal-rich rings were observed on both freeze-dried (Sarret *et al.*, 2002; Isaure *et al.*, 2006; Fukuda *et al.*, 2008) and frozen-hydrated trichomes (Küpper *et al.*, 2000; Zhao *et al.*, 2000; Isaure *et al.*, 2006), and a more homogeneous distribution of metals at the base of the trichomes was observed on both freeze-dried (Ager *et al.*, 2003) and frozen-hydrated (Hokura *et al.*, 2006) trichomes. The fact that some trichomes did not present metal enrichments is also intriguing. This might be related to their age, or to their position on the leaf.

Based on a Cd enrichment in the asperities present on the cuticle of *Arabidopsis* trichomes and on a predominance of O/N ligands for this metal, Isaure *et al.* (2006) proposed that the metal was mostly located in the cell wall and cuticle. Fukuda *et al.* (2008) also found O/N ligands for cadmium in the trichomes of *A. halleri* ssp. *gemmifera*. We previously found that Zn was fourfold coordinated and complexed to carboxyl and/or hydroxyl groups in *A. halleri* trichomes (Sarret *et al.*, 2002). The results obtained in the present study consistently show that phosphate, thiol and silanol groups can be excluded as major Zn ligands in *A. halleri* trichomes, based on the low amount of P, S and Si in the Zn-rich region. It is clearly established that metals accumulated in leaf cells follow the symplasmic pathway (Verbruggen *et al.*, 2009), so the metals present in the cell wall of trichomes likely transit through the cytoplasm of these cells. Indeed, an enhancement of sulfur metabolism was observed in *A. thaliana* trichomes under metal exposure (Guo *et al.*, 2003; Howarth *et al.*, 2003). The excretion of Zn through glandular trichomes has been shown in the case

of tobacco (*Nicotiana tabacum*; Sarret *et al*., 2006 and references therein), whereas the possible transport or excretion of this metal in the extracellular compartment of non glandular trichomes has not been documented.

In summary, the present study on *A. halleri*, *A. lyrata* and selected F_1 and F_2 progenies showed a correlation between Zn accumulation in the leaves and the proportion of Zn–OAs + Zn_{aq}, corresponding to octahedrally coordinated Zn. The vein/leaf tissue fluorescence ratio was negatively correlated with Zn accumulation, which is consistent with an enhanced transfer of Zn from the vascular tissues to the mesophyll and/or epidermis. The higher proportion of Zn–OAs + Zn_{aq} and the depletion of the veins in the stronger accumulators suggest that xylem unloading and vacuolar sequestration in the leaves are related to Zn hyperaccumulation. Finally, elemental distributions observed in the trichomes of *A. halleri* and *A. lyrata* are consistent with an association of Zn with organic compounds, most likely the polysaccharides of the cell wall.

Acknowledgements

This research was supported by the French Programme ACI/FNS/ECCO (ECODYN, contract no. 04 2 9 FNS) and by the Nord-Pas-de-Calais Region, 'Programme de Recherches Concertées'. The operations of the Advanced Light Source at Lawrence Berkeley National Laboratory are supported by the Director, Office of Science, Office of Basic Energy Sciences, US Department of Energy under contract number DE-AC02-05CH11231. We acknowledge J. L. Hazemann and O. Proux for their assistance during EXAFS measurements. The authors thank the ESRF (Grenoble, France) and the ALS (Berkeley, USA) for the provision of beamtime.

References

Ager FJ, Ynsa MD, Dominguez Solis JR, Lopez Martin MC, Gotor C, Romero LC. 2003. Nuclear micro-probe analysis of *Arabidopsis thaliana* leaves. *Nuclear Instruments and Methods in Physics Research Section B* **210**: 401–406.

Becher M, Talke IN, Krall L, Kramer U. 2004. Cross-species microarray transcript profiling reveals high constitutive expression of metal homeostasis genes in shoots of the zinc hyperaccumulator *Arabidopsis halleri*. *Plant Journal* **37**: 251–268.

Bert V, Meerts P, Saumitou-Laprade P, Salis P, Gruber W, Verbruggen N. 2003. Genetic basis of Cd tolerance and hyperaccumulation in *Arabidopsis halleri*. *Plant and Soil* **249**: 9–18.

Broadley MR, White PJ, Hammond JP, Zelko I, Lux A. 2007. Zinc in plants. *New Phytologist* **173**: 677–702.

Brune A, Urbach W, Dietz K-J. 1994. Compartmentation and transport of zinc in barley primary leaves as basic mechanisms involved in zinc tolerance. *Plant, Cell & Environment* **17**: 153–162.

Chiang HC, Lo JC, Yeh KC. 2006. Genes associated with heavy metal tolerance and accumulation in Zn/Cd hyperaccumulator *Arabidopsis halleri*: a genomic survey with cDNA microarray. *Environmental Science and Technology* **40**: 6792–6798.

Deniau AX, Pieper B, Ten Bookum WM, Lindhout P, Aarts MGM, Schat H. 2006. QTL analysis of cadmium and zinc accumulation in the heavy metal hyperaccumulator *Thlaspi caerulescens*. *Theoretical and Applied Genetics* **113**: 907–920.

Drager DB, Desbrosses-Fonrouge AG, Krach C, Chardonnens AN, Meyer RC, Saumitou-Laprade P, Kramer U. 2004. Two genes encoding *Arabidopsis halleri* MTP1 metal transport proteins co-segregate with zinc tolerance and account for high MTP1 transcript levels. *Plant Journal* **39**: 425–439.

Dräger DB, Voigt K, Kramer U. 2005. Short transcript-derived fragments from the metal hyperaccumulator model species *Arabidopsis halleri*. *Zeitschrift Fur Naturforschung C a Journal of Biosciences* **60**: 172–178.

Ebbs S, Zambrano M, Spiller S, Newville M. 2009. Cadmium sorption, influx and efflux at the mesophyll layer of leaves from ecotypes of the Zn/Cd hyperaccumulator *Thlaspi caerulescens*. *New Phytologist* **181**: 626–636.

Elbaz B, Shoshani-Knaani N, David-Assael O, Mizrachy-Dagri T, Mizrahi K, Saul H, Brook E, Berezin I, Shaul O. 2006. High expression in leaves of the zinc hyperaccumulator *Arabidopsis halleri* of AhMHX, a homolog of an *Arabidopsis thaliana* vacuolar metal/proton exchanger. *Plant, Cell & Environment* **29**: 1179–1190.

Filatov V, Dowdle J, Smirnoff N, Ford-Lloyd B, Newbury HJ, Macnair MR. 2007. A quantitative trait loci analysis of zinc hyperaccumulation in *Arabidopsis halleri*. *New Phytologist* **174**: 580–590.

Frérot H, Lefèbvre C, Petit C, Collin C, Dos Santos A, Escarré J. 2005. Zinc tolerance and hyperaccumulation in F_1 and F_2 offspring from intra and interecotype crosses of *Thlaspi caerulescens*. *New Phytologist* **165**: 111–119.

Frey B, Keller C, Zierold K, Schulin R. 2000. Distribution of Zn in functionally different leaf epidermal cells of the hyperaccumulator *Thlaspi caerulescens*. *Plant, Cell & Environment* **23**: 675–687.

Fukuda N, Hokura A, Kitajima N, Terada Y, Saito H, Abed T, Nakai A. 2008. Micro X-ray fluorescence imaging and micro X-ray absorption spectroscopy of cadmium hyper-accumulating plant, *Arabidopsis halleri* ssp. *gemmifera*, using high-energy synchrotron radiation. *Journal of Analytical Atomic Spectrometry* **23**: 1068–1075.

Guo WJ, Bundithya W, Goldsbrough PB. 2003. Characterization of the Arabidopsis metallothionein gene family: tissue-specific expression and induction during senescence and in response to copper. *New Phytologist* **159**: 369–381.

Hanikenne M, Talke IN, Haydon MJ, Lanz C, Nolte A, Motte P, Kroymann J, Weigel D, Kramer U. 2008. Evolution of metal hyperaccumulation required *cis*-regulatory changes and triplication of HMA4. *Nature* **453**: 391–395.

Hassinen VH, Tuomainen M, Peraniemi S, Schat H, Karenlampi SO, Tervahauta AI. 2009. Metallothioneins 2 and 3 contribute to the metal-adapted phenotype but are not directly linked to Zn accumulation in the metal hyperaccumulator, *Thlaspi caerulescens*. *Journal of Experimental Botany* **60**: 187–196.

Hokura A, Onuma R, Kitajima N, Terada Y, Saito H, Abe T, Yoshida S, Nakai I. 2006. 2-D X-ray fluorescence imaging of cadmium hyperaccumulating plants by using high-energy synchrotron radiation X-ray microbeam. *Chemistry Letters* **35**: 1246–1247.

Howarth JR, Dominguez Solis JR, Gutierrez Alcala G, Wray JL, Romero LC, Gotor C. 2003. The serine acetyltransferase gene family in *Arabidopsis thaliana* and the regulation of its expression by cadmium. *Plant Molecular Biology* **51**: 589–598.

Isaure MP, Fayard B, Sarret G, Pairis S, Bourguignon J. 2006. Localization and chemical forms of cadmium in *Arabidopsis thaliana*. *Spectrochimica Acta Part B* **61**: 1242–1252.

Kistenmacher T. 1972. A refinement of the structure of *bis*-(L-histidinato)zinc(II) dihydrate. *Acta Crystallographica B* **28**: 1302–1304.

Koch MA, Matschinger M. 2007. Evolution and genetic differentiation among relatives of *Arabidopsis thaliana*. *Proceedings of the National Academy of Sciences, USA* **104**: 6272–6277.

Küpper H, Kroneck PMH. 2005. Heavy metal uptake by plants and cyanobacteria. In: Sigel A, Sigel H, Sigel R, eds. *Metal ions in biological systems*, Vol. 44. New York, NY, USA: Marcel Dekker, 97–142.

Küpper H, Zhao FJ, McGrath SP. 1999. Cellular compartmentation of zinc in leaves of the hyperaccumulator *Thlaspi caerulescens*. *Plant Physiology* **119**: 305–311.

Küpper H, Lombi E, Zhao FJ, McGrath SP. 2000. Cellular compartmentation of cadmium and zinc in relation to other elements in the hyperaccumulator *Arabidopsis halleri*. *Planta* **212**: 75–84.

Küpper H, Mijovilovich A, Meyer-Klaucke W, Kroneck PMH. 2004. Tissue- and age-dependent differences in the complexation of cadmium and zinc in the cadmium/zinc hyperaccumulator *Thlaspi caerulescens* (Ganges ecotype) revealed by X-ray absorption spectroscopy. *Plant Physiology* **134**: 748–757.

Lasat MM, Baker AJM, Kochian LV. 1998. Altered Zn compartmentation in the root symplasm and stimulated Zn absorption into the leaf as mechanisms involved in Zn hyperaccumulation in *Thlaspi caerulescens*. *Plant Physiology* **118**: 875–883.

Lobinski R, Moulin C, Ortega R. 2006. Imaging and speciation of trace elements in biological environment. *Biochimie* **88**: 1591–1604.

Macnair M. 2002. Within and between population genetic variation for zinc accumulation in *Arabidopsis halleri*. *New Phytologist* **155**: 59–66.

Macnair MR, Bert V, Huitson SB, Saumitou-Laprade P, Petit D. 1999. Zinc tolerance and hyperaccumulation are genetically independent characters. *Proceedings of the Royal Society of London B* **266**: 2175–2179.

Marcus MA, MacDowell AA, Celestre R, Manceau A, Miller T, Padmore HA, Sublett RE. 2004. Beamline 10.3.2 at ALS: a hard X-ray microprobe for environmental and materials sciences. *Journal of Synchrotron Radiation* **11**: 239–247.

Martell AE, Smith RM. 1982. *Critical stability constants*. New York, NY, USA: Plenum Press.

Palmgren M, Clemens S, Williams L, Krämer U, Borg S, Schjørring J, Sanders D. 2008. Zinc biofortification of cereals: problems and solutions. *Trends in Plant Science* **13**: 464–473.

Panfili F, Manceau A, Sarret G, Spadini L, Kirpichtchikova T, Bert V, Laboudigue A, Marcus M, Ahamdach N, Libert M. 2005. The effect of phytostabilization on Zn speciation in a dredged contaminated sediment using scanning electron microscopy, X-ray fluorescence, EXAFS spectroscopy and principal components analysis. *Geochimica et Cosmochimica Acta* **69**: 2265–2284.

Parkhurst DL, Appelo CAJ. 1999. User's guide to PhreeqC (version 2) A computer program for speciation batch-reaction, one dimensional transport and inverse geochemical calculations. *In U.S. Geological Survey Water-Resources Investigations Report* N° 99–4259.

Pauwels M, Saumitou-Laprade P, Holl A, Petit D, Bonnin I. 2005. Multiple origin of metallicolous populations of the pseudometallophyte *Arabidopsis halleri* (Brassicaceae) in central Europe: the cpDNA testimony. *Molecular Ecology* **14**: 4403–4414.

Pauwels M, Frérot H, Bonnin I, Saumitou-Laprade P. 2006. A broad-scale analysis of population differentiation for Zn tolerance in an emerging model species for tolerance study: *Arabidopsis halleri* (Brassicaceae). *Journal of Evolutionary Biology* **19**: 1838–1850.

Ravel B, Newville M. 2005. ATHENA and ARTEMIS: interactive graphical data analysis using IFEFFIT. *Journal of Synchrotron Radiation* **12**: 537–541.

Reed AT, Karipides A. 1976. The crystal structure of S-Malatodiaquozinc(II) hydrate. *Acta Crystallographica* **B32**: 2085.

Rehr JJ, Mustre de Leon J, Zabinsky SI, Albers RC. 1991. Theoretical X-ray absorption fine structure standards. *J. Am. Chem. Soc.* **113**: 5135–5145.

Richau K, Schat H. 2009. Intraspecific variation of nickel and zinc accumulation and tolerance in the hyperaccumulator *Thlaspi caerulescens*. *Plant and Soil* **314**: 253–262.

Richau K, Kozhevnikova A, Seregin I, Vooijs R, Koevoets PLM, Smith A, Ivanov V, Schat H. 2009. Chelation by histidine inhibits the vacuolar sequestration of nickel in roots of the hyperaccumulator *Thlaspi caerulescens*. *New Phytologist* **183**: 106–116.

Roosens N, Willems G, Saumitou-Laprade P. 2008a. Using Arabidopsis to explore zinc tolerance and hyperaccumulation. *Trends in Plant Science* **13**: 208–215.

Roosens N, Willems G, Gode C, Courseaux A, Saumitou-Laprade P. 2008b. The use of comparative genome analysis and syntenic relationships allows extrapolating the position of Zn tolerance QTL regions from *Arabidopsis halleri* into *Arabidopsis thaliana*. *Plant and Soil* **306**: 105–116.

Salt DE, Prince RC, Baker AM, Raskin I, Pickering IJ. 1999. Zinc ligands in the metal hyperaccumulator *Thlaspi caerulescens* as determined using X-ray absorption spectroscopy. *Environmental Science and Technology* **33**: 713–717.

Salt DE, Prince RC, Pickering IJ. 2002. Chemical speciation of accumulated metals in plants: evidence from X-ray absorption spectroscopy. *Microchemical Journal* **71**: 255–259.

Sarret G, Manceau A, Spadini L, Roux JC, Hazemann JL, Soldo Y, Eybert-Bérard L, Menthonnex JJ. 1998. EXAFS determination of Pb, Zn complexing sites of *Penicillium chrysogenum* cell walls. *Environmental Science and Technology* **32**: 1648–1655.

Sarret G, Saumitou-Laprade P, Bert V, Proux O, Hazemann JL, Traverse A, Marcus MA, Manceau A. 2002. Forms of zinc accumulated in the hyperaccumulator *Arabidopsis halleri*. *Plant Physiology* **130**: 1815–1826.

Sarret G, Balesdent J, Bouziri L, Garnier JM, Marcus MA, Geoffroy N, Panfili F, Manceau A. 2004. Zn speciation in the organic horizon of a contaminated soil by micro X-ray fluorescence, micro and powder EXAFS spectroscopy and isotopic dilution. *Environmental Science and Technology* **38**: 2792–2801.

Sarret G, Harada E, Choi YE, Isaure MP, Geoffroy N, Birschwilks M, Clemens S, Fakra S, Marcus MA, Manceau A. 2006. Trichomes of tobacco excrete zinc as Zn-substituted calcium carbonate and other Zn-containing compounds. *Plant Physiology* **141**: 1021–1034.

Talke IN, Hanikenne M, Kramer U. 2006. Zinc-dependent global transcriptional control, transcriptional deregulation, and higher gene copy number for genes in metal homeostasis of the hyperaccumulator *Arabidopsis halleri*. *Plant Physiology* **142**: 148–167.

Terzano R, Al Chami Z, Vekemans B, Janssens K, Miano T, Ruggiero P. 2008. Zinc distribution and speciation within rocket plants (*Eruca vesicaria* L. Cavalieri) grown on a polluted soil amended with compost as determined by XRF microtomography and Micro-XANES. *Journal of Agricultural and Food Chemistry* **56**: 3222–3231.

Ueno D, Ma JF, Iwashita T, Zhao FJ, McGrath SP. 2005. Identification of the form of Cd in the leaves of a superior Cd-accumulating ecotype of *Thlaspi caerulescens* using Cd-113-NMR. *Planta* **221**: 928–936.

Van Belleghem F, Cuypers A, Semane B, Smeets K, Vangronsveld J, d'Haen J, Valcke R. 2007. Subcellular localization of cadmium in roots and leaves of *Arabidopsis thaliana*. *New Phytologist* **173**: 495–508.

Van Steveninck RFM, Barbare A, Fernando DR, Van Steveninck ME. 1994. The binding of zinc, but not cadmium, by phytic acid in roots of crop plants. *Plant and Soil* **167**: 157–164.

Van-Rossum F, Bonnin I, Fenart S, Pauwels M, Petit D, Saumitou-Laprade P. 2004. Spatial genetic structure within a metallicolous population of *Arabidopsis halleri*, a clonal, self-incompatible and heavy-metal-tolerant species. *Molecular Ecology* **13**: 2959–2967.

Vazquez MD, Barcelo J, Poschenrieder C, Madico J, Hatton P, Baker AJM, Cope GH. 1992. Localization of zinc and cadmium in *Thlaspi caerulescens* (Brassicaceae), a metallophyte that can hyperaccumulate both metals. *Journal of Plant Physiology* **140**: 350–355.

Verbruggen N, Hermans C, Schat H. 2009. Molecular mechanisms of metal hyperaccumulation in plants. *New Phytologist* **181**: 759–776.

Weber M, Harada E, Vess C, von Roepenack Lahaye E, Clemens S. 2004. Comparative microarray analysis of *Arabidopsis thaliana* and *Arabidopsis halleri* roots identifies nicotianamine synthase, a ZIP transporter and other genes as potential metal hyperaccumulation factors. *Plant Journal* **37**: 269–281.

Whitaker A. 1975. The crystal structure of Hopeite, $Zn_3(PO_4)_2$, $4H_2O$. *Acta Crystallographica* **31**: 2026–2035.

Willems G, Dräger D, Courbot M, Godé C, Verbruggen N, Saumitou-Laprade P. 2007. The genetic basis of zinc tolerance in the metallophyte *Arabidopsis halleri* ssp. *halleri* (Brassicaceae): an analysis of quantitative trait loci. *Genetics* **176**: 659–674.

Xing JP, Jiang RF, Ueno D, Ma JF, Schat H, McGrath SP, Zhao FJ. 2008. Variation in root-to-shoot translocation of cadmium and zinc among different accessions of the hyperaccumulators *Thlaspi caerulescens* and *Thlaspi praecox*. *New Phytologist* **178**: 315–325.

Zha HG, Jiang FJ, Zhao FJ, Vooijs R, Schat H, Barker JHA, McGrath SP. 2004. Co-segregation analysis of cadmium and zinc accumulation in *Thlaspi caerulescens* interecotypic crosses. *New Phytologist* **163**: 299–312.

Zhao F, Lombi E, Breedon T, McGrath S. 2000. Zinc hyperaccumulation and cellular distribution in *Arabidopsis halleri*. *Plant, Cell & Environment* **23***: 507–514.*

Supporting Information

Additional supporting information may be found in the online version of this article.

Methods S1. Preparation of zinc (Zn) model compounds.

Fig. S1 (a) K-edge extended X-ray absorption fine structure (EXAFS) spectra for aqueous zinc (Zn) reference compounds; (b) Zn K-edge EXAFS spectra for aqueous Zn^{2+}, Zn citrate and Zn + 3 organic acids (OAs) in solution, Zn–cell wall and ZnPhos.

Fig. S2 Micro X-ray fluorescence (μXRF) maps of a trichome of *Arabidopsis halleri* also presented in Fig. 10.

Fig. S3 Micro X-ray fluorescence (μXRF) maps of a trichome of *Arabidopsis lyrata* also presented in Fig. 10.

Fig. S4 Micro X-ray fluorescence (μXRF) maps of trichome of $F_{2–3}$ also presented in Fig. 10.